

Spatio-Temporal Consistent Soft Sensor Modeling and Monitoring of Thermal Power Plants based on Physical Knowledge

Qianchao Wang¹, Peng Sha², Leena Heistrene³, Yuxuan Ding^{1†}, Yaping Du¹,

Abstract—Data-driven soft sensors have been widely applied in complex industrial processes. However, the interpretable spatio-temporal features extraction by soft sensors remains a challenge. In this light, this work introduces a novel method termed spatio-temporal consistent and interpretable model (STCIM). First, temporal and spatial features are captured and aligned by a far topological spatio-temporal consistency extraction block. Then, the features are mapped into an interpretable latent space for further prediction by explicitly giving physical meanings to latent variables. The efficacy of the proposed STCIM is demonstrated through the modeling of two generated datasets and a real-life dataset of coal-fired power plants. The corresponding experiments show: 1) The generalization of STCIM outperforms other methods, especially in different operation situations. 2) The far topological spatio-temporal consistency is vital for feature alignment. 3) The hyper-parameters of physics-informed interpretable latent space loss decide the performance of STCIM.

Keywords—Power plant, Soft sensor, Deep-learning, physics-informed modeling

I. INTRODUCTION

TO reduce carbon emissions and mitigate the greenhouse effect, the modeling and monitoring of thermal power plants become the cornerstones of stable operation and security in the energy system. However, data offset, noise disturbance, low reliability of analyzers, and delays in long time-series data from most processes lead to a mismatch between models and the data, resulting in potential safety hazards and poor product quality. As a solution, soft sensors are used for process monitoring, quality prediction, and many other important applications in thermal power plants [1].

There are two main types of approaches to establish soft sensing models, namely, mechanism-based methods [2] and data-driven methods [3], [4]. Mechanism-based methods, also called first-principle models, use physicochemical governing equations and dynamic differential equations to describe industrial processes [5], [6]. It can model or monitor thermal power plants in an interpretable and reliable way. When we

have sufficient knowledge about thermal power plants and the process, mechanism-based methods can work effectively, improving practitioners' trust in the models. However, the complexity of thermal power plants often makes these preconditions difficult to meet, limiting the applicability of the first principles. In contrast, data-driven methods, particularly deep learning (DL), have achieved significant success in chemical, biochemical, and metallurgical processes, since they do not require extensive prior knowledge [7]–[9].

In recent research, deep learning methods have been increasingly applied to large-scale industrial processes, with a particular emphasis on spatio-temporal feature extraction to capture both spatial dependencies and temporal dynamics among variables [10]. These approaches build on foundational techniques such as multiscale information fusion [11] and dynamic feature extraction [12], but prioritize spatio-temporal integration to address complex interactions. Some efforts focused on local spatio-temporal features [13], incorporating mechanisms like BiGRU with attention for time-related patterns [14] and dynamic convolutional neural networks with multiscale attention for hierarchical local nonlinear dynamics [15]. However, the far topological structures in industrial variables often limit local methods, prompting advancements in broader spatio-temporal modeling [16]. For instance, variable correlation analysis-based convolutional neural networks have been proposed to extract far topological spatio-temporal features in processes like hydrocracking and debutanizer columns [17]. Similarly, spatio-temporal attention combined with long short-term memory networks identifies long-term variable correlations in hydrocracking [18], while graph neural networks process relational structures for enhanced spatio-temporal feature extraction [19]. However, many learned broader spatio-temporal features assume alignment across space and time, overlooking delays and couplings among variables, which can lead to reduced generalization in real-world applications. This problem is particularly evident in thermal power plants and needs to be solved.

Another problem is that black-box models lack physical interpretability, critical for safety in thermal power plants. Sparse spatio-temporal features in long time-series data are not explainable by first principles, limiting their utility. While graph neural networks incorporate prior knowledge to identify physical correlations [10], [20], they lack explicit physical grounding. Physics-informed neural networks (PINNs) address this by embedding physical laws into loss functions via differential equations and initial conditions, leveraging automatic

Yuxuan Ding is the corresponding author

¹ Qianchao Wang, Yuxuan Ding, and Yaping Du is with the Department of Building Environment and Energy Engineering, Hong Kong Polytechnic University, Hung Hom, Hong Kong. (qianchao.wang@polyu.edu.hk; yx.ding@connect.polyu.hk; Ya-ping.du@polyu.edu.hk)

² Peng Sha is with Key Laboratory of Energy Thermal Conversion and Control of Ministry of Education, School of Energy and Environment, Southeast University, Nanjing, China. (sha_peng@seu.edu.cn)

³ Leena Heistrene is with Department of Electrical Engineering, School of Energy Technology, Pandit Deendayal Energy University, Gandhinagar, Gujarat, India. (leena.santosh@sof.pdpu.ac.in)

differentiation for transparency [21]–[23]. Successful applications include lake temperature prediction [24], parameter estimation [25], and flexibility analysis [26]. Despite advantages in efficiency, noise immunity, and accuracy, PINNs implicitly encode physical properties, lacking explicit expressions of these relationships.

Considering this gap, the primary objective of this study is to introduce an explicitly interpretable spatio-temporally consistent soft sensor model in thermal power plant modeling and monitoring. We propose a spatio-temporal consistent and interpretable model (STCIM) with a spatio-temporal consistent feature extraction block and an interpretable latent space. This method unfolds in two distinct phases: in the first stage, a root layer is designed to extract the local features at different times, and a trainable position encoding layer is embedded into the root layer to ensure the local spatio-temporal consistency. Subsequently, the local consistent features are utilized as the input to a far topological alignment layer, computing the correlations among the features by attention mechanism. During the process, the position encoding layer can adaptively update itself to ensure the consistency of far topological spatio-temporal features. In the second stage, the spatio-temporal consistent features are projected into the latent space. The latent space is guided by the first principle, explicitly assigning physical meanings to maintain the interpretability of the model. In training process, the latent space is integrated into the loss function to predict the state variables and the output. Notably, this methodology holds potential for adaptation to other domains within industrial modeling or diagnostic applications. The efficacy of these concepts is validated through extensive experimentation using simulated datasets and real-world data from a 330MW thermal power plant. In summary, the key contributions of this paper encompass:

- 1) A spatio-temporal consistent and interpretable model (STCIM) is proposed for thermal power plant modeling and monitoring. It efficiently extracts and aligns the spatio-temporal features and gives the latent variables physical meanings to improve the model's interpretability.
- 2) The spatio-temporal consistent feature extraction block is introduced to extract and align local and global spatio-temporal features by using trainable position encoding and attention modules.
- 3) The physics-informed interpretable latent space loss function is introduced to map the latent space into the state variables by giving explicit physical meanings to latent space and integrating them in a discrete state-space loss function. The discrete state-space loss function is a part of the physics-informed interpretable latent space loss function.
- 4) The efficacy of STCIM is underscored through its application experiments and ablation experiments in two simulated datasets and two real thermal power plant datasets, thus substantiating its effectiveness in practical settings.

The paper is organized as follows: Section II provides background about the thermal power plant, basic blocks,

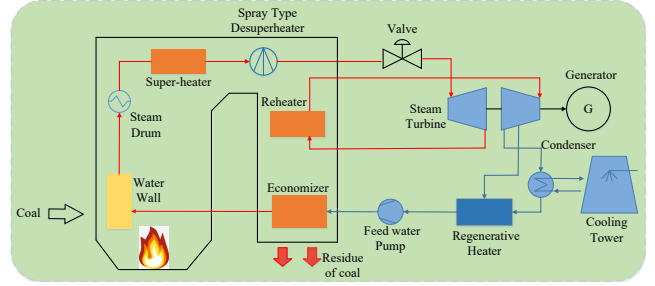


Fig. 1. 330MW thermal power plant.

and physics-informed loss functions. Section III describes the detailed information of the proposed STCIM, including the model structure, the spatio-temporal consistent feature extraction block, and physics-informed interpretable latent space loss function. Section IV shows the experimental results, and Section V concludes the paper.

II. BRIEF INTRODUCTION OF THERMAL POWER PLANTS

Thermal power plant is a multifaceted and complex industrial process, generating electricity by converting heat energy from fossil fuels into electrical energy [27]. It contains the chemical reactions, energy conversion, mass transfer which is shown in Fig. 1. The process begins with fuel combustion in a boiler, producing high-pressure steam that drives a turbine connected to a generator, which produces electricity. After passing through the turbine, the steam is cooled in a condenser and recycled, while the exhaust gases are treated and released through a chimney.

The mathematical description of the utilized 330MW thermal power plant [28], [29] can be given by

$$\begin{aligned}
 r'_B &= e^{-18s} u_B \\
 120 \frac{dr_B}{dt} &= -r_B + r'_B \\
 3266 \frac{dp_d}{dt} &= -0.2501 p_t u_T + 6.77 r_B \\
 12 \frac{dN_E}{dt} &= -N_E + 0.2501 p_t u_T \\
 p_t &= p_d - 0.0004555 (6.77 r_B)^{1.3}
 \end{aligned} \tag{1}$$

where u_B is the fuel signal (kg/s), u_T is the opening of turbine (%), r_B is the actual fuel (kg/s), p_d is the pressure of steam (MPa) and N_E is the output power (MW). $\dot{z}_1 = \frac{dr_B}{dt}$, $\dot{z}_2 = \frac{dp_d}{dt}$ and $\dot{y} = \frac{dN_E}{dt}$ (z_1, z_2 are the state variables). It is derived from the first principles of the thermal power plant.

III. SPATIO-TEMPORAL CONSISTENT AND INTERPRETABLE MODELING

Modern multi-coupled industrial processes involve interconnected production units with complex material and energy transfers, posing challenges in modeling and monitoring due to time delays, variable coupling, and interpretability. We developed a trainable position coding to align spatio-temporal consistency during local and far topological feature extraction. Additionally, we designed a physics-informed interpretable latent space loss function by assigning physical meanings to

latent variables and incorporating them into the loss function. This section details the STCIM, focusing on the spatio-temporal consistent feature extraction block and the physics-informed interpretable latent space loss function.

A. Model Structure

Fig. 2 (a) shows the flow chart of the proposed STCIM. It can be recognized as an encoder-decoder structure, in which the spatio-temporal consistent feature extraction block (encoder) is divided into two sub-blocks: the local spatio-temporal consistent feature extraction block and the far topological alignment block, and the decoder is a fully connected network.

In the local spatio-temporal consistent feature extraction block, the temporal features are extracted by the kernels with different size. The trainable position layer is added in parallel to temporal feature extraction as the position embedding to ensure the consistency of local spatio-temporal features. Then the local features are utilized to calculate the far topological correlations based on the attention mechanism, capturing the coupling among features in the far topological alignment block. During the process, the position encoding can adaptively update itself based on the new captured coupling features to ensure the consistency of far topological spatio-temporal features.

The latent space is another important node, which is utilized to explicitly add physical meanings to models. The spatio-temporal consistent features are projected into the latent space and constrained by the first principles by adding a discrete state-space loss in the physic-informed interpretable latent space loss function. The size of the latent space is determined by the form of discrete state-space equations, e.g., if there are two state variables in a discrete model, then the number of latent variables for STCIM is four because it contains the state variables at time k and $k - 1$. The decoder is composed of MLPs, which is enough for discrete function fitting.

In general, the idea of the model can be summarized as compressing the spatio-temporal consistent features with high dimensions into an interpretable latent space, which normally has fewer dimensions, and then the interpretable latent variables are utilized to fit the potential mathematical equations, for example, the state-space equations.

B. Spatio-Temporal Consistent Feature Extraction Block

The spatio-temporal consistent feature extraction block mainly focuses on the consistency of space and time in features by designing a trainable position encoding layer. It contains the local spatio-temporal consistent feature extraction block and the far topological alignment block. In the two blocks, during the training process, the position encoding layer can adaptively update itself to ensure the spatio-temporal consistency in any features.

1) *Local Spatio-Temporal Feature Extraction Block*: Fig. 2 (b) describes the local spatio-temporal feature extraction block. The input data, respectively, pass through a temporal feature extraction layer and a trainable position encoding layer to capture the local features from different times and locations. The

massive local spatio-temporal features ensure the abundance of far topological variables.

Assume that the input variables at time t are $X(t) \in R^{H \times W \times C}$ where H , W , and C are separately the backtracking from time t , the number of features, and the number of input channels ($C = 1$). $X(t)$ can be expressed as

$$X(t) = \begin{bmatrix} x_1(t - (H - 1) \times T) & x_2(t - (H - 1) \times T) & \cdots & x_n(t - (H - 1) \times T) \\ \vdots & \vdots & \vdots & \vdots \\ x_1(t - 2 \times T) & x_2(t - 2 \times T) & \cdots & x_n(t - 2 \times T) \\ x_1(t - 1 \times T) & x_2(t - 1 \times T) & \cdots & x_n(t - 1 \times T) \\ x_1(t) & x_2(t) & \cdots & x_n(t) \end{bmatrix} \quad (2)$$

where T is the sampling time. When different convolution kernels are applied in $X(t)$, the local features of adjacent attributes and times $S_{i,j}$ are extracted, reflecting the dynamics of the industrial process, $S_{i,j} = \sum_{m=1}^m \sum_{n=1}^n K_{m,n} X(t)_{i+m,j+n} + b$.

However, this kind of one-shot input is disorder, ignoring the potential position information in attributes, which is opposite to the clear production procedures of the industrial process. Therefore, we designed a trainable position encoding layer, providing the corresponding spatial features to ensure the consistency of spatio-temporal features. Inspired by [30], the trainable position encoding layer is given by

$$Position_j = \frac{Variable_j}{\sqrt{N}} \quad (3)$$

where $Variable_j$ is the trainable position parameter of j_{th} attributes. N is the number of features that is a scaling factor. $Position_j$ is the position encoding of the j_{th} attributes. Due to the unknown time delay and coupling among variables in industrial processes, fixed position encoding is not appropriate, for example, 'sin' and 'cos' encoding. The trainable position parameter $Variable_j$ in this layer can adaptively ensure spatio-temporal consistency of captured local features. The final local spatio-temporal consistent features can be summarized as

$$\hat{S}_j = S_j + Position_j \quad (4)$$

where \hat{S}_j is the final feature of j_{th} attributes.

2) *Far Topological Alignment Block*: During the industrial process, variables are related not only to adjacent nodes but also to variables in far topological structures. Aligning the far topological correlation among local features and making sure the spatio-temporal consistency are vital for the modeling and monitoring of thermal power plant. In this vein, we propose a far topological alignment block, which is shown in Fig. 2 (c).

The local spatio-temporal consistent features are first sparsely mapped by the multi-head linear transformations to highlight different aspects of the features. Then several self-attention modules are utilized to capture the far topological structure in features by calculating the attention weights of all features. The calculated weights can be considered as the dependencies among far topological features and captured by models. Subsequently, the captured topological and spatio-temporal features pass through a fully connected module with GeLU to provide nonlinear properties. In the forward process, there are two shortcut connections to ensure the flow of information. During the far topological variable correlation

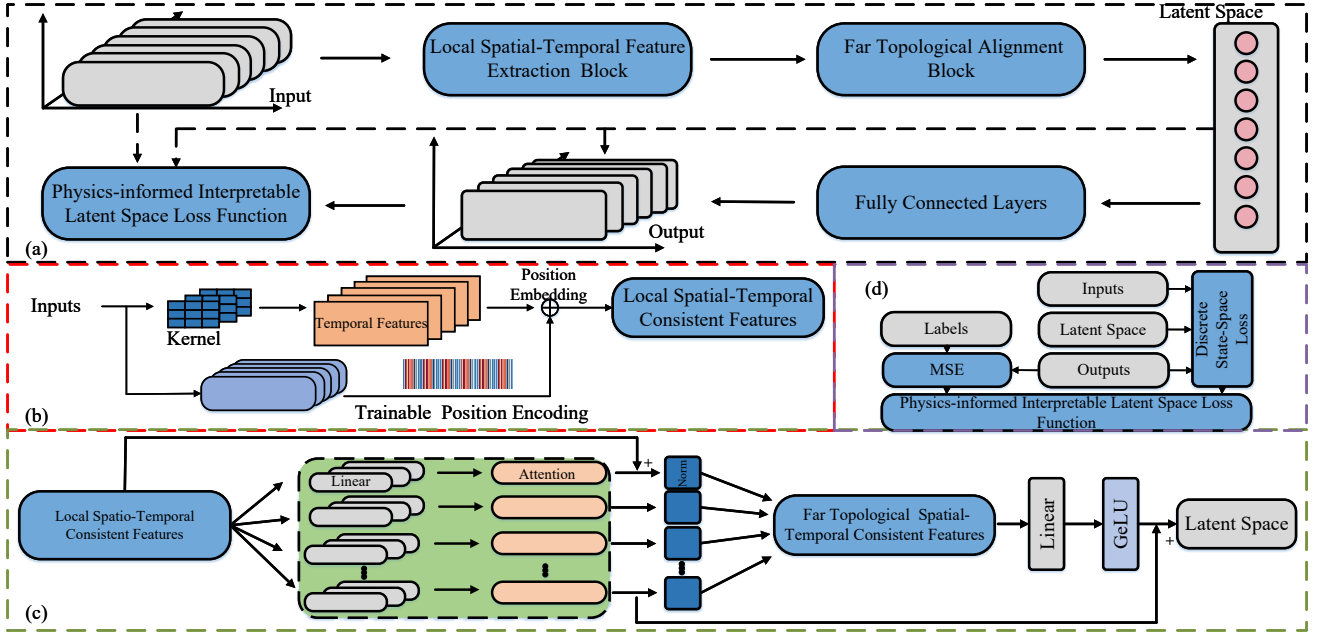


Fig. 2. Overview of the STCIM framework. (a) The flow chart of STCIM. (b) The local spatio-temporal feature extraction block. (c) The far topological alignment block. (d) The physics-informed interpretable latent space loss function

extraction process, the adaptive position encoding at the local spatio-temporal feature extraction layer is realigned with new features, which will again ensure the consistency of the far topological spatio-temporal feature and improve the modeling and monitoring accuracy.

Assume that the features captured by the local spatio-temporal feature extraction block are $\hat{S} \in R^{H \times W \times K}$. Based on the attention weights, the dependencies among far topological features can be calculated by

$$Weight(\hat{S}, \hat{S}) = SoftMax\left(\frac{\hat{S}\hat{S}^T}{\sqrt{d_k}}\right) \quad (5)$$

$$S_{new} = Weight(\hat{S}, \hat{S})\hat{S} \quad (6)$$

where $Q = K = V = \hat{S}$. The calculated weights determine the intrinsic correlation among the input features, helping the networks capture the potential far topological structure among all the features. By multiplying $Weight(\hat{S}, \hat{S})$ with \hat{S} , the importance determined by the long-term topological correlation can be used in feature extraction.

C. Physics-informed Interpretable Latent Space Loss Function

To map these sparse spatio-temporal consistent features into an interpretable latent space and limit the space in first principles, this subsection introduces the physics-informed interpretable latent space loss function by giving physical meanings to the latent space z of STCIM and adding them to the discrete state-space loss, which is shown in Fig. 2 (d). We can directly relate the inputs, latent variables, and outputs by the discrete state-space loss function and boundary conditions. Here, we need to highlight that the latent space z is an intermediate process parameter instead of the input of STCIM. It can be unobserved or hard to measure.

Assuming the discrete-time state-space equation and output equation of the industrial process are given by

$$u(t) = \Phi(u(t-1), \theta_1) + G(x(t), \theta_2) \quad (7)$$

$$y(t) = H(u(t), \theta_3) + J(x(t), \theta_4) \quad (8)$$

where x is the input, u is the unobserved state variables, and y is the output. $\Phi(\cdot), G(\cdot), H(\cdot), J(\cdot)$ are separately the nonlinear operators. θ is the parameter. All variables are vectors.

Now, we can map the discrete-time state-space equation into STCIM by defining the latent variables with state variables in Eq. (7). Assuming that the latent space z of STCIM is the state variables at time $t-1$ and t ($z_1 = u(t), z_2 = u(t-1)$) and $z = [z_1, z_2]$ and the input and output of the STCIM are x and \hat{y} , respectively. Then, the discrete state-space loss function can be given by

$$Loss_{state} = \gamma_1(\hat{y} - H(z_1, \theta_3) - J(x, \theta_4)) + \gamma_2(z_1 - \Phi(z_2, \theta_1) - G(x, \theta_2)) \quad (9)$$

where γ is the weight coefficient. The discrete state-space loss function is used to constrain the latent variables to follow the state-space equations, i.e. the underlying laws of physics. By adding it to the MSE loss, we get the physics-informed interpretable latent space loss function, given by

$$Loss = L(y, \hat{y}) + \lambda R(\theta) + Loss_{state} \quad (10)$$

When $\gamma = [\gamma_1, \gamma_2] \rightarrow \infty$, the STCIM completely trusts the state-space model. In contrast, when $\gamma = [\gamma_1, \gamma_2] \rightarrow 0$, the STCIM is a data-driven model without physical prior knowledge. Assuming that the devices follow a unified nonlinear model across different operating conditions, the optimal γ is certain and determined by whether this model can be trusted, i.e., how simplified the state-space model is. By balancing the tendencies towards data-driven and physics-driven

models, STCIM can achieve the trade-off in the loss function. According to Eq. (10), the physics-informed interpretable latent space loss function consists of four sub-losses: 1) the MSE loss $L(y, \hat{y})$, 2) the parametric regularization of the model $R(\theta)$, 3) the output equation loss $\hat{y} - H(z_1, \theta_3) - J(x, \theta_4)$, 4) the state equation loss $z_1 - \Phi(z_2, \theta_1) - G(x, \theta_2)$. Although the state variables are not measurable, the neural network will output the actual state variables due to the latent space being constrained at both sub-losses 3 and 4, which provides physical properties.

IV. EXPERIMENTAL RESULTS

To validate the efficiency of our method, we test the proposed STCIM in three stages. First, analytical experiments based on two generated datasets are used to demonstrate the effectiveness of STCIM. Then, a real-life dataset from a 330MW power plant is utilized as a comparative experiment to further validate the robustness and efficiency of STCIM. The scalability of STCIM is tested using a dataset from 1000MW ultra-supercritical once-through boiler-turbine unit. At last, we emphasize the importance of position encoding, far topological coupling among variables, and hyper-parameters in the loss function.

A. Experiment Setup

The two generated datasets include a rotor equation-reduced rotary speed dataset and a 3-order synchronous generator dataset, which are both important for the equipment of thermal power plant. The comparative experiment has 330MW and 1000MW coal-fired power plant datasets that reflects a complex industrial process with heat and mass transformation. All the datasets have two operation conditions, and each condition has at least 50,000 points with noise. The model is trained in one operation condition and tested in another to highlight the effectiveness of STCIM. The state variables are not used as input to models.

For each STCIM block, we have different parameters. In the local spatio-temporal feature extraction layer block, the features are extracted by two 2D-convolution layers with 8 filters, and each kernel is 3×3 . The far topological alignment layer has four heads, and each head has three linear transformations, and each linear layer has 32 neurons. The number of interpretable variables is chosen based on the real physical model. For the decoder, each fully connected layer has 32 neurons and GeLU as an activation function. For all experiments, γ_1 and γ_2 in Eq. (9) are set as 1 and 0.5 separately. During the training process, the latent variables and the target output of STCIM will be integrated into the discrete state-space loss function and then collaboratively optimized by the backpropagation algorithm.

The STCIM is composed of two sub-blocks with computationally intensive expressions: the local spatio-temporal feature extraction block and the far topological alignment block. For the attribute size of input, $X(t) \in R^{H \times W \times C}$, the computation will intensify in the local spatio-temporal feature extraction block by $\mathcal{O}(K^2 \times C \times M \times H \times W)$ factor, where the K is the kernel size, M is the number of output channels of

TABLE I
THE PRM OF MAIN MODELS. #PRM DENOTES THE NUMBER OF PARAMETERS.

Models	STCIM	PhyLSTMs [26]	PIML [31]	VCACNN [17]
#PRM	0.023M	0.428M	0.025M	0.371M
Models	MSACNN [15]	MIAN [11]	TimeVAE [32]	-
#PRM	0.082M	0.012M	0.302M	-

the block. Similarly, the computation complexity of the far topological alignment block is $\mathcal{O}(D \times B \times H \times (W^2 + H \times W + W \times m))$, where D is the total number of attention layers and feedforward layers, B is the batch size, m is the hidden dimension of the MLP. Since the local spatio-temporal feature extraction block only contains the two 2D-convolution layers, the computational complexity of STCIM is mainly affected by far topological alignment block which contains attention and feedforward layers. The attention mechanism's $\mathcal{O}(H^2 \times W)$ term may be significant for long sequences, while the $\mathcal{O}(W^2)$ term dominates for large model dimensions.

Six more deep learning-based soft sensor modeling methods are explored for comparisons, including PhyLSTM [26], PIML [31], MSACNN [15], VCACNN [17], MIAN [11], and TimeVAE [32]. The six methods include the PINN-based interpretable models and the CNN-based, attention-based, and VAE-based spatiotemporal features extraction models. They have demonstrated their out-performance in different soft sensor of large-scale industrial processes. Table I shows the number of parameters of models. For each experiment, we train the models with a batch size of 64 or 128 using the 'NAdam' optimizer with an initialized learning rate of 0.01. The learning rate decays by a factor of 0.1 every 30 epochs. The max epoch is set to 100. The experiments are implemented in Tensorflow using a CPU Intel i7-11800H CPU at 2.3Hz and an NVIDIA T600 GPU.

B. Analytical Experiments

In this section, we use two widely used equipment models in thermal power plants to demonstrate the reliability and scalability of STCIM in modeling and condition monitoring. For the evaluation, we use MAE, MSE and MAPE as the indicators.

1) *Rotor Equation-Reduced Rotary Speed*: The stability of the rotor is one of the key factors for the stable operation of thermal power plants. During the operation, the rotor needs to maintain a certain speed and stability to ensure the normal operation of the machine and avoid the damage to the machine. The reduced rotary speed can be given by

$$\begin{aligned} \frac{dn}{dt} &= \frac{900}{\pi^2 J n} (N_T - N_C), \\ \hat{n} &= \frac{n}{\sqrt{\frac{T_1}{288}}} \end{aligned} \quad (11)$$

where n is the rotor speed, J is the rotary inertia, \hat{n} is the output reduced rotary speed, T_1 is the air temperature and N_T and N_C are separately the generated power by the turbines and consumed power by the compressor. The generated dataset

TABLE II
EVALUATION METRICS OF THE 3-ORDER SYNCHRONOUS GENERATOR

Evaluation		STCIM	PhyLSTMs [26]	PIML [31]	VCACNN [17]	MSACNN [15]	MIAN [11]	TimeVAE [32]
MAE (10^{-2})	i_q	3.38	3.45	3.57	3.41	3.66	3.52	3.69
	i_d	3.63	4.07	4.23	3.78	4.05	3.95	4.07
	w	9.18	16.94	12.51	10.27	11.03	10.54	14.12
	\hat{E}_q	1.46	1.45	1.47	1.42	1.33	1.40	1.42
MSE (10^{-3})	i_q	1.75	1.79	1.88	1.80	1.99	1.83	1.94
	i_d	2.08	2.55	2.73	2.62	2.72	2.65	2.71
	w	13.12	46.30	57.13	36.78	18.05	25.45	39.78
	\hat{E}_q	0.32	0.35	0.34	0.35	0.36	0.36	0.36
MAPE	i_q	4.15%	4.24%	4.38%	4.26%	4.47%	4.34%	4.51%
	i_d	27.03%	28.44%	29.32%	28.01%	27.21%	27.68%	27.46%
	w	9.18%	16.93%	17.29%	16.87%	11.02%	15.48%	13.98%
	\hat{E}_q	1.52%	1.52%	1.48%	1.51%	1.49%	1.50%	1.49%

contains all the inputs, outputs, and states with 80,000 points with noise.

Fig 3 shows that in a simple equipment monitoring, the STCIM completely outperforms all other models, including the physics-based and feature extraction-based models. First, the conventional fully connected network is not enough to extract the necessary features, resulting in the worst performance of PIML. Then, the time-related features can improve the forecasting precision, which is reflected in PhyLSTM and TimeVAE. Due to the limited variables and the fast characteristics, the local or the global spatio-temporal features in the rotor equation are similar, which makes the performances of VCACNN, MSACNN, and MIAN similar. However, in this experiment, the underlying physical laws in PhyLSTM and PIML do not improve the accuracy of state variable estimation, which may be due to the simplicity of the models.

2) *3 Order Synchronous Generator*: The synchronous generator is the core equipment in the thermal power system, responsible for converting mechanical energy into electrical energy. Its stable operation is directly related to the reliability and safety of the entire power system. We use the classic 3-order synchronous generator as the simulation model, which is given as follows for data generation.

$$\begin{aligned}
 T'_{do} \frac{d\hat{E}_q}{dt} &= E_f - \hat{E}_q - (x_d - x'_d)i_d, \\
 T_J \frac{dw}{dt} &= P_m - [\hat{E}_q i_q - (x'_d - x_q)i_d i_q], \\
 \frac{d\delta}{dt} &= w - 1, \\
 u_d &= x_q i_q - r_a i_d, \\
 u_q &= \hat{E}_q - x'_d i_d - r_a i_q.
 \end{aligned} \tag{12}$$

where i is the input current, u is the output voltage, w is the angular velocity, and \hat{E}_q is the transient internal voltage. Since δ is not related to outputs, it will be ignored in our case. Other parameters are constants. The generated dataset contains all the generated currents, voltages, angular velocity and power with 50,000 points for each operation condition.

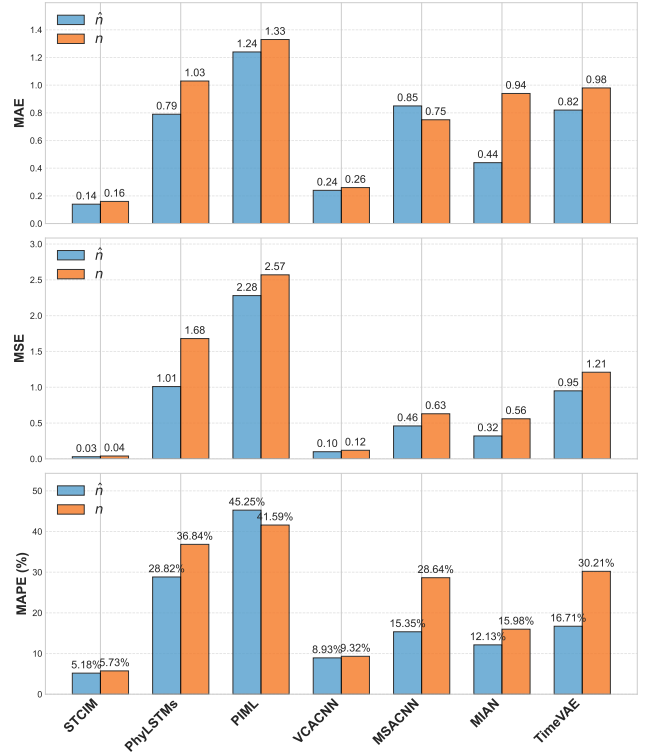


Fig. 3. Evaluation metrics of rotor equation reduced rotary speed.

Table II shows the evaluation of the state estimation (w , \hat{E}_q) and the output regression (i_q , i_d). The proposed STCIM outperforms the other deep learning methods in most evaluation metrics, especially in the output regression and w estimation. Compared to other models, the performance of \hat{E}_q estimation of STCIM is competitive as well. The bias in the latent variable \hat{E}_q may be caused by the hyper-parameter γ_2 of loss function. Considering the good performance of w estimation and that the dataset of 3rd order synchronous generator is generated, the hyper-parameter γ_2 can be set larger for better performance. Similar to fig 3, due to the local or global spatio-temporal feature extraction, VCACNN, MSACNN, and MIAN have better performance than PhyLSTM, PIML, and TimeVAE.

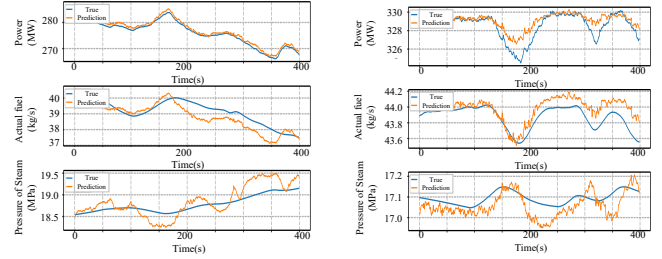
As the complexity of the model increases, accurate feature extraction becomes increasingly important. Another interesting thing is that the regression accuracy of state estimation (w, \hat{E}_q) of PhyLSTM and PIML is becoming competitive, which is different from Fig 3. We need to emphasize that the regression of state estimation (w, \hat{E}_q) of PhyLSTM and PIML is unsupervised, since we add the discrete state-space loss in the final loss function like STCIM. They are fundamentally different from VCACNN, MSACNN, MIAN, and TimeVAE.

C. Comparative Experiments

This section is used to demonstrate the effectiveness of STCIM in a real thermal power plant. We collect the dataset from a real 330MW thermal power plant, which follows the introduction in Section II. In the dataset, there are two operating conditions and 13 features, and each feature has 96,000 points with noise. The generalization of STCIM is tested under both the same operation condition (Test 1) and a different operation condition (Test 2).

1) *The comparisons of different methods*: Table III summarizes the evaluation metrics of all models in both Test 1 and Test 2. At the same operating point, the performance of the models varies, which might be caused by the size of models, the different captured features. For models that only focus on local features (MSACNN), the performance is almost the worst when predicting the output and the state variables at the same time. For long time-series data, the models related time-related features (PhyLSTM and TimeVAE) outperform MSACNN, indicating the importance of long-term characteristics in the data. In PIML, time as input and domain decomposition help it achieve good performance, especially the output forecasting. Models with spatio-temporal feature achieve the best performance among all models, including STCIM, VCACNN, and MIAN. Benefiting from the built-in physics-informed interpretable latent space loss function, STCIM has more accurate state variable monitoring without labels. However, in another operating point, the generalization of STCIM is much better than that of other models. An interesting thing is that the generalization of the physic-informed models (PhyLSTM and PIML) in this experiment is better than other feature extraction-based models, especially the state variables forecasting. It indicates that when the thermal power plant follows unified physical laws, embedding the physical information is equivalent to extracting the intrinsic spatio-temporal features, without complex network architecture, which helps the model to generalize more easily.

2) *The visualization of output and interpretable latent variables*: Fig. 4 shows the output forecasting and state estimation (interpretable latent variables) of the real thermal power plant dataset using STCIM. To reveal the performance of STCIM, 400 points in the test dataset are selected in the figures, including Test 1 and Test 2. Although the performance of STCIM in output forecasting in Test 1 is not the best, it still closely follows the actual value. Compared with Fig. 4a, the performance of STCIM in Fig. 4b is better, owing to the obvious fluctuations in state variables, the detailed information from sub-devices, and the physic-informed loss function. Therefore,



(a) Test 1 of the real thermal power plant dataset (b) Test 2 of the real thermal power plant dataset

Fig. 4. The output forecasting and state variables monitoring of comparative experiments

as well as the spatio-temporal feature consistency, the explicit interpretable latent space along with the physic-informed loss function helps STCIM maintain a good generalization ability in prediction and monitoring under a new operating point.

3) *The scalability of STCIM: 1000MW Thermal Power Plant*: To demonstrate that STCIM can be applied to other thermal power plants, we use a real dataset from a 1000MW ultra-supercritical once-through boiler-turbine unit [33]. The inputs are separately the fuel signal (kg/s), total water flow (kg/s), turbine valve opening (%). The latent variables (z_1, z_2) are separately the steam-water separator pressure (MPa) and the steam-water separator enthalpy (kJ/kg). The outputs (y_1, y_2) are the main steam pressure (MPa) and the output power (MW). Each features has 96,000 points with noise.

Fig 5 summarizes the evaluation metrics of all models when tested under a different operation condition. STCIM outperforms other models in this experiment. Since the process of the 1000MW ultra-supercritical once-through boiler-turbine unit is more complex than that of the 330MW thermal power plant, the differences between the models are more significant. The integrated physical information loss function forces the models (STCIM, PhyLSTM, and PIML) to satisfy the first principles, which improves the generalization ability of the models, especially in steam-water separator enthalpy forecasting. Instead of extracting spatio-temporal features from a single operation condition, the additional loss and the adopted spatio-temporal consistency can provide more potential physical information to ensure the safety of thermal power plants.

D. Ablation Experiments

In this section, we discuss the importance of spatio-temporal consistency and the hyper-parameters of the physics-informed interpretable latent space block in STCIM. The real-life dataset of 330MW thermal power plant is utilized in ablation experiments. The setup is the same as in comparative experiments.

1) *The importance of adaptive position encoding*: Table IV shows the evaluation metrics of Test 1 and Test 2 without adaptive position encoding. Compared with Table III, there is a slight decrease in the output forecasting and variable estimation, indicating the effectiveness of spatio-temporal consistency. Whereas, the difference is not remarkable. In contrast, the generalization of STCIM without adaptive position encoding in Test 2 is worse compared to the performance of STCIM

TABLE III
EVALUATION METRICS OF THE REAL-LIFE DATASET

Evaluation		STCIM	PhyLSTMs [26]	PIML [31]	VCACNN [17]	MSACNN [15]	MIAN [11]	TimeVAE [32]
MAE (Test 1)	y	0.45	0.41	0.40	0.46	0.78	0.51	0.58
	z_1	0.43	0.76	0.61	0.44	1.07	0.67	0.92
	z_2	0.18	0.21	0.69	0.18	0.51	0.35	0.49
MSE (Test 1)	y	0.31	0.29	0.26	0.31	1.01	0.52	0.65
	z_1	0.25	0.87	0.59	0.29	1.73	0.46	0.98
	z_2	0.05	0.08	1.71	0.06	0.43	0.26	0.37
MAPE (Test 1)	y	0.37%	0.26%	0.25%	0.45%	0.78%	0.52%	0.76%
	z_1	1.20%	1.98%	1.58%	1.12%	2.77%	1.69%	2.35%
	z_2	0.98%	1.12%	1.61%	0.99%	2.66%	1.32%	2.03%
MAE (Test 2)	y	0.46	0.54	0.57	0.46	0.75	0.59	0.66
	z_1	0.11	0.56	0.14	0.28	0.68	0.32	0.58
	z_2	0.05	0.05	1.38	0.11	0.26	0.18	0.22
MSE (Test 2)	y	0.49	0.50	0.67	1.08	0.94	0.92	0.87
	z_1	0.02	0.07	0.03	0.05	0.07	0.07	0.06
	z_2	0.03	0.04	0.07	0.16	0.09	0.12	0.10
MAPE (Test 2)	y	0.14%	0.15%	0.21%	0.48%	0.23%	0.37%	0.29%
	z_1	0.35%	0.65%	0.35%	0.44%	0.55%	0.48%	0.52%
	z_2	0.33%	0.34%	0.54%	0.67%	0.61%	0.65%	0.62%

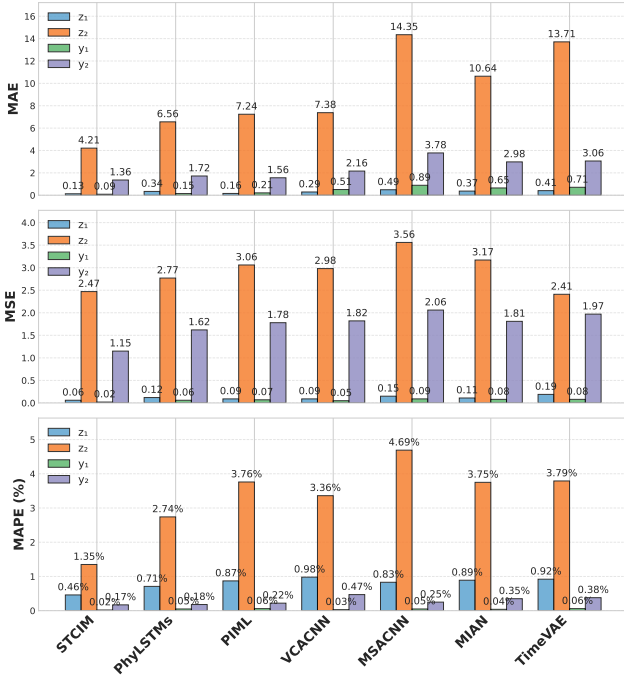


Fig. 5. Evaluation metrics of 1000MW thermal power plant.

in Table III. For example, the MSE in y forecasting without adaptive position encoding almost triples compared with STCIM with adaptive position encoding. The improvement of generalization benefits from adaptive position encoding. By position encoding, the features are endowed with additional information, which improves the expressiveness of STCIM.

2) *The importance of far topological alignment:* Table V describes how the evaluation metrics change when the far topological alignment is replaced by a CNN model. Different

TABLE IV
EVALUATION METRICS OF EXPERIMENTS IN REAL-LIFE DATASET WITHOUT POSITION ENCODING

Datasets	MSE			MAE			MAPE		
	y	z_1	z_2	y	z_1	z_2	y	z_1	z_2
Test 1	0.83	0.35	0.06	0.81	0.47	0.15	0.38%	1.20%	1.12%
Test 2	1.37	0.06	0.06	0.98	0.21	0.09	2.90%	1.48%	0.54%

TABLE V
EVALUATION METRICS OF EXPERIMENTS IN A REAL-LIFE DATASET WITHOUT FAR TOPOLOGICAL ALIGNMENT

Datasets	MSE			MAE			MAPE		
	y	z_1	z_2	y	z_1	z_2	y	z_1	z_2
Test 1	0.97	0.42	0.06	0.90	0.51	0.32	0.46%	1.38%	1.45%
Test 2	1.78	0.13	0.09	1.08	0.32	0.09	2.93%	1.56%	0.82%

from the comparisons in Table IV, the performance of STCIM at both Test 1 experiment is greatly affected, especially in the y prediction and z_1 estimation, which means that for complex thermal power plants and coupled variables, global and topological features are more important. In Test 2 experiment, the performance becomes worse, due to the change of operating point. The lack of far topological alignment makes the model focus more on local features, while ignoring the potential dependencies of far topological correlations of variables, reducing the accuracy of modeling and monitoring, which is fatal for a large and complex industrial process.

3) *Sensitivity analysis of hyper-parameters γ in Test 2:* The impact of hyper-parameters γ_1 and γ_2 on performance of STCIM are tested. Fig. 6 shows the performance of STCIM using different γ . When the discrete state-space loss (Fig.(6a)) is not considered in final loss function, STCIM becomes a supervised output and state variables forecasting like VCACNN and the forecasting is unable to align with actual data even

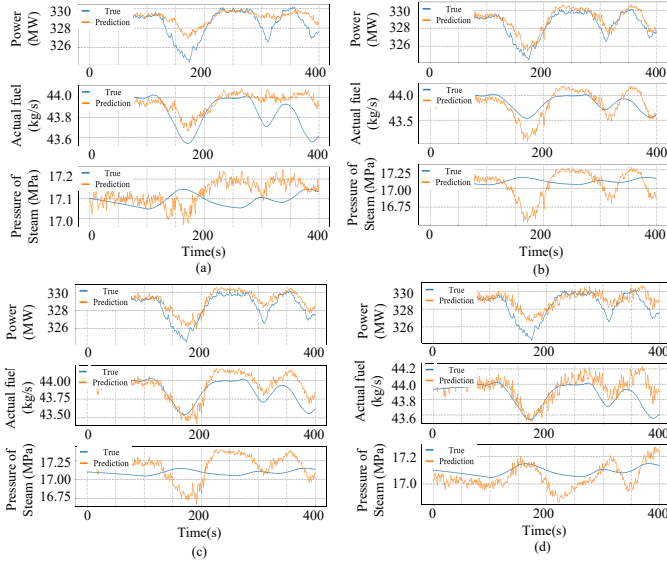


Fig. 6. Sensitivity analysis of hyper-parameters γ_1 and γ_2 in Test 2 using thermal power plant dataset. (a) $\gamma_1 = 0$ and $\gamma_2 = 0$. (b) $\gamma_1 = 1$ and $\gamma_2 = 0$. (c) $\gamma_1 = 0$ and $\gamma_2 = 1$. (d) $\gamma_1 = 1$ and $\gamma_2 = 1$.

though the trend is similar. In Figs.(6b) and (6c), the utilized part of the discrete state-space loss can partly guarantee the fit of state variables. Due to the strong correlation between the state variables and the output, actual fuel and pressure of steam follow the trend of output power, which is different from the actual values. In Fig.(6d), the pressure of steam follows the trend of the real values, due to all the discrete state-space equations are used as part of the loss function.

TABLE VI
EVALUATION METRICS OF EXPERIMENTS WITH DIFFERENT INPUT DIMENSION

Datasets	MSE			MAE			MAPE		
	y	z_1	z_2	y	z_1	z_2	y	z_1	z_2
H=5	0.82	0.06	0.11	0.62	0.22	0.13	0.28%	0.47%	0.58%
H=10	0.56	0.03	0.09	0.51	0.14	0.07	0.17%	0.41%	0.40%
H=20	0.49	0.02	0.03	0.46	0.11	0.05	0.14%	0.35%	0.33%

4) *The impact of input dimension H in Test 2:* Table VI discusses the impact of input dimension H on the performance of STCIM ($Input \in R^{H \times W \times C}$). Due to the limited computational resources, we test three different H . When the backtracking is small, the advantages of STCIM is hard to see. The inner far topological consistent spatio-temporal feature is replaced by the local spatio-temporal feature, making the performance of STCIM comparable to that of CNN-based models. As H increases, the performance of STCIM is further enhanced. However, considering the computational complexity of STCIM in attention mechanism, a larger H will bring more burden to the device.

V. CONCLUSION

As modern industrial processes become complex, general soft sensor methods are gradually unable to meet the requirements. This paper introduces a novel soft sensor method termed spatio-temporal consistent and interpretable model (STCIM). We designed a spatio-temporal consistent feature

extraction block to capture and align local and global temporal and spatial features from raw data. Subsequently, by giving physical meanings to latent variables and integrating them in a physics-informed interpretable latent space loss function, the latent space maps the spatio-temporal consistent features to an interpretable latent variables to improve the model interpretability. The primary outcome underscores the capability to effectively extract and align the spatio-temporal features and the interpretability of STCIM. The analytical and comparative experiments underscore that STCIM has robust generalization performance across diverse operational conditions, particularly when the training dataset exhibits significant fluctuations in both outputs and state variables, thereby enabling informed and reliable decision-making among power domain experts. The ablation experiments highlight the critical significance of adaptive position encoding, the far topological alignment, and the hyper-parameters of the loss function.

The key limitation of the approach lies in its dependence on prior knowledge of the loss function. When more intricate state-space equations are incorporated into the model, part of the equations can lead to gradient disappearance. Nonetheless, we believe that STCIM has considerable potential for explicitly elucidating the neural network operations. Therefore, there may be significant room for future research, which may focus on the combination of physical models and neural networks.

REFERENCES

- [1] Y. Jiang, S. Yin, J. Dong, and O. Kaynak, "A review on soft sensors for monitoring, control, and optimization of industrial processes," *IEEE Sensors J.*, vol. 21, no. 11, pp. 12 868–12 881, 2021.
- [2] B. Huang, Y. Qi, and A. M. Murshed, *Dynamic modeling and predictive control in solid oxide fuel cells: first principle and data-based approaches*. Wiley, 2013.
- [3] X. Yuan, N. Xu, L. Ye, K. Wang, F. Shen, Y. Wang, C. Yang, and W. Gui, "Attention-based interval aided networks for data modeling of heterogeneous sampling sequences with missing values in process industry," *IEEE Trans. Ind. Informat.*, vol. 20, no. 4, pp. 5253–5262, 2024.
- [4] R. Guo, H. Liu, G. Xie, Y. Zhang, and D. Liu, "A self-interpretable soft sensor based on deep learning and multiple attention mechanism: From data selection to sensor modeling," *IEEE Trans. Ind. Informat.*, vol. 19, no. 5, pp. 6859–6871, 2023.
- [5] A. Mukherjee, V. Saini, S. Adeyemo, D. Bhattacharyya, D. Purdy, J. Parker, and C. Boohaker, "Development of hybrid first principles-artificial intelligence models for transient modeling of power plant superheaters under load-following operation," *Appl. Therm. Eng.*, vol. 262, p. 124795, 2025.
- [6] B. van Veldhuizen, L. van Biert, C. Ünlübayir, K. Visser, J. Hopman, and P. V. Aravind, "Component sizing and dynamic simulation of a low-emission power plant for cruise ships with solid oxide fuel cells," *Energy Convers. Manag.*, vol. 326, p. 119477, 2025.
- [7] Q. Wang, L. Pan, J. Shen, and N. Lu, "Power plant data filtering based on gaussian naive bayesian classification and prediction error method," in *2019 Chinese Automation Congress (CAC)*, 2019, pp. 1490–1495.
- [8] Q. Sun and Z. Ge, "A survey on deep learning for data-driven soft sensors," *IEEE Trans. Ind. Informat.*, vol. 17, no. 9, pp. 5853–5866, 2021.
- [9] X. Zhang, C. Song, J. Zhao, and B. Huang, "Fault-tolerant soft sensor modeling based on a two-dimensional group distributionally robust optimization framework," *IEEE Trans. Autom. Sci. Eng.*, vol. 22, pp. 14 396–14 406, 2025.
- [10] L. Ma, M. Wang, and K. Peng, "A spatiotemporal industrial soft sensor modeling scheme for quality prediction with missing data," *IEEE Trans. Instrum. Meas.*, vol. 73, pp. 1–10, 2024.
- [11] J. Xue, K. Li, T. Zhang, and H. Ye, "Data-driven soft sensor for hot strip mill process based on multiscale information-fusion attention network," *IEEE Trans. Instrum. Meas.*, vol. 73, pp. 1–11, 2024.

- [12] C. F. Lui, Y. Liu, and M. Xie, "A supervised bidirectional long short-term memory network for data-driven dynamic soft sensor modeling," *IEEE Trans. Instrum. Meas.*, vol. 71, pp. 1–13, 2022.
- [13] Y. Zhao, X. Deng, J. Zhang, and P. Wang, "Spatio-temporal regularized stochastic configuration network for supervised and semi-supervised soft sensor development," *IEEE Trans. Autom. Sci. Eng.*, vol. 22, pp. 10960–10972, 2025.
- [14] S. Zou, K. Li, Z. Li, F. Huang, and L. Chen, "A soft sensor model based on rime-tcn-bigru-attention for predicting heavy calcium carbonate particle size distribution," *IEEE Trans. Instrum. Meas.*, vol. 74, pp. 1–13, 2025.
- [15] X. Yuan, L. Huang, L. Ye, Y. Wang, K. Wang, C. Yang, W. Gui, and F. Shen, "Quality prediction modeling for industrial processes using multiscale attention-based convolutional neural network," *IEEE Trans. Cybern.*, vol. 54, no. 5, pp. 2696–2707, 2024.
- [16] X. Shi, R. Li, H. Morales, A. Amicarelli, W. Huang, and W. Xiong, "Semi-supervised probabilistic learning network for soft sensor modeling with partially labeled data," *IEEE Trans. Autom. Sci. Eng.*, vol. 22, pp. 16309–16321, 2025.
- [17] X. Yuan, Y. Wang, C. Wang, L. Ye, K. Wang, Y. Wang, C. Yang, W. Gui, and F. Shen, "Variable correlation analysis-based convolutional neural network for far topological feature extraction and industrial predictive modeling," *IEEE Trans. Instrum. Meas.*, vol. 73, pp. 1–10, 2024.
- [18] X. Yuan, L. Li, Y. A. W. Shardt, Y. Wang, and C. Yang, "Deep learning with spatiotemporal attention-based lstm for industrial soft sensor model development," *IEEE Trans. Ind. Electron.*, vol. 68, no. 5, pp. 4404–4414, 2021.
- [19] Z. Yang, L. Mao, L. Ye, Y. Ma, Z. Song, and Z. Chen, "Akgnn: When adaptive graph neural network meets kolmogorov-arnold network for industrial soft sensors," *IEEE Trans. Instrum. Meas.*, vol. 74, pp. 1–13, 2025.
- [20] L. Kong, C. Yang, S. Lou, Y. Cai, X. Huang, and M. Sun, "Collaborative extraction of intervariable coupling relationships and dynamics for prediction of silicon content in blast furnaces," *IEEE Trans. Instrum. Meas.*, vol. 72, pp. 1–13, 2023.
- [21] M. Raissi, P. Perdikaris, and G. Karniadakis, "Physics-informed neural networks: A deep learning framework for solving forward and inverse problems involving nonlinear partial differential equations," *J. Comput. Phys.*, vol. 378, pp. 686–707, 2019. [Online]. Available: <https://www.sciencedirect.com/science/article/pii/S0021999118307125>
- [22] H. Meskhidze, "Beyond classification and prediction: The promise of physics-informed machine learning in astronomy and cosmology," February 2024, forthcoming in: Juan Durán and Giorgia Pozzi (Eds.) *Philosophy of Science for Machine Learning: Core Issues and New Perspective*, Synthese Library. [Online]. Available: <https://philsci-archive.pitt.edu/23067/>
- [23] B. Huang and J. Wang, "Applications of physics-informed neural networks in power systems - a review," *IEEE Trans. Power Syst.*, vol. 38, no. 1, pp. 572–588, 2023.
- [24] A. Daw, A. Karpatne, W. D. Watkins, J. S. Read, and V. Kumar, "Physics-guided neural networks (pgnn): An application in lake temperature modeling," in *Knowledge guided machine learning*. Chapman and Hall/CRC, 2022, pp. 353–372.
- [25] W. Wang and N. Yu, "Estimate three-phase distribution line parameters with physics-informed graphical learning method," *IEEE Trans. Power Syst.*, vol. 37, no. 5, pp. 3577–3591, 2022.
- [26] M. Lahariya, F. Karami, C. Develder, and G. Crevecoeur, "Physics-informed lstm network for flexibility identification in evaporative cooling system," *IEEE Trans. Ind. Informat.*, vol. 19, no. 2, pp. 1484–1494, 2023.
- [27] M. Fan, Y. Zhao, Z. Liu, Z. Wang, M. Liu, and J. Yan, "Dynamic modelling and thermo-mechanical performance evaluation of thermal power plants during the background of enhanced operational flexibility," *Energy*, vol. 318, p. 134943, 2025.
- [28] Q. Wang, L. Pan, Z. Liu, H. Wang, X. Wang, and W. Tang, "Interpretable uncertainty forecasting framework for robust configuration of energy storage in a virtual power plant," *JEnergyStorage*, vol. 84, p. 110800, 2024. [Online]. Available: <https://www.sciencedirect.com/science/article/pii/S2352152X24003840>
- [29] Q. Wang, L. Pan, and K. Y. Lee, "Improving superheated steam temperature control using united long short term memory and mpc," *IFAC-PapersOnLine*, vol. 53, no. 2, pp. 13345–13350, 2020.
- [30] A. Dosovitskiy, L. Beyer, A. Kolesnikov, D. Weissenborn, X. Zhai, T. Unterthiner, M. Dehghani, M. Minderer, G. Heigold, S. Gelly, *et al.*, "An image is worth 16x16 words: Transformers for image recognition at scale," *arXiv preprint arXiv:2010.11929*, 2020.
- [31] J. Kruse, E. Cramer, B. Schäfer, and D. Witthaut, "Physics-informed machine learning for power grid frequency modeling," *PRX energy*, vol. 2, no. 4, p. 043003, 2023.
- [32] B. Shen, X. Jiang, L. Yao, and J. Zeng, "Gaussian mixture timevae for industrial soft sensing with deep time series decomposition and generation," *J. Process Control*, vol. 147, p. 103355, 2025.
- [33] H. Fan, Z.-g. Su, P.-h. Wang, and K. Y. Lee, "A dynamic nonlinear model for a wide-load range operation of ultra-supercritical once-through boiler-turbine units," *Energy*, vol. 226, p. 120425, 2021.